# Density functional study of the structural, electronic, and vibrational properties of $\beta$-$Ba_2TiO_4$

William D. Parker*
*Argonne Leadership Computing Facility, Argonne National Laboratory, Argonne, Illinois 60439, USA*
*and School of Chemical Engineering, Purdue University, West Lafayette, Indiana 47907, USA*

S. M. Nakhmanson
*Department of Materials Science & Engineering, and Institute of Materials Science,*
*University of Connecticut, Storrs, Connecticut 06269, USA*

(Received 17 June 2013; revised manuscript received 27 September 2013; published 6 December 2013)

Motivated by the reported high dielectric response of monoclinic $\beta$-$Ba_2TiO_4$ as well as its affinity for absorbing small molecules, we investigate its structural, electronic, and vibrational properties with density functional theory (DFT). DFT-based structural optimization obtains lattice parameters and bond lengths within a few percent of experimentally observed values, with specific details depending on the choice of exchange-correlation functional. Although, for both the local density approximation (LDA) and generalized gradient approximation (GGA) functionals employed, the DFT calculations produce a wide-band-gap insulating state for $\beta$-$Ba_2TiO_4$ (with an indirect gap of 4.1 eV or greater), they do not agree on the energetic ordering of this phase with respect to its perovskite-like Ruddlesden-Popper (RP) polymorph. Simulations that utilize LDA place the $\beta$ phase 0.30 eV higher, while those using the Perdew-Burke-Ernzerhof GGA functional place it 0.22 eV lower than the RP one, leaving the question of the degree of perovskite-like phase metastability under epitaxial growth conditions unresolved. Comparison of the formula unit volumes of the $A_2TiO_4$ and $ATiO_3$ polymorphs ($A$ = Sr, Ba) reveals that both $Ba_2TiO_4$ structures possess much more open geometries—more so for the $\beta$ than for the RP phase—than their isostoichiometric Sr-based counterparts and all of the examined $ATiO_3$ compounds, in line with the demonstrated propensity of the Ba-based 2-1-4 oxides to capture molecules like $CO_2$ and $H_2O$. However, an analysis of vibrations and their contributions to the static dielectric permittivity tensor of $\beta$-$Ba_2TiO_4$ indicates that, unlike the perovskite RP phase, this structure does not exhibit strong polar lattice distortions, which results in a rather low value for its average static dielectric constant.

DOI: 10.1103/PhysRevB.88.245108 PACS number(s): 77.84.Cg, 63.20.dk, 77.22.Ch, 71.15.Mb

## I. INTRODUCTION

$Ba_2TiO_4$ is the only stable ternary compound in the Ba-rich region of the BaO-$TiO_2$ phase diagram at concentrations of greater than two thirds of BaO.[1,2] The low-temperature $\beta$ phase of $Ba_2TiO_4$ is a monoclinic structure of $\beta$-$K_2SO_4$ prototype with space group $P2_1/n$[3] while the high temperature $\alpha'$ phase has orthorhombic $P2_1nb$ symmetry.[4] These structures are unusual among ternary titanates because Ti and O ions arrange themselves in a tetrahedron, rather than an octahedron, which is typical for perovskitelike materials. For example, in the same orthotitanate stoichiometry, the Sr-based compound forms a Ruddlesden-Popper (RP) structure with a tetragonal $I4/mmm$ symmetry.[5] $Ba_{2-x}Sr_xTiO_4$ solid solutions synthesized by a variety of ceramic techniques have also been investigated, but a single-phase RP compound with any substantial concentration of Ba has not been realized. Instead, either mixtures of monoclinic and RP phases, or, for Ba-rich compounds, single phases containing $Sr^{2+}$ substitutions into the prototypical $\beta$-$K_2SO_4$ structure are obtained.[6,7]

$\beta$-$Ba_2TiO_4$ can be produced both in ceramic[8–11] and thin film forms.[12,13] Its mixed $\beta$-$\alpha'$-phase crystals exhibit high dielectric permittivity (950 at 1 MHz),[8] suggesting potential applications as high-$\kappa$ dielectric materials. In addition, $\beta$-$Ba_2TiO_4$ displays a remarkable propensity for absorbing and desorbing (in a reversible fashion) small molecules and has recently been evaluated as a prospective material for high-temperature (550 °C and above) $CO_2$ capture.[14–16] Other Ba-based structures of the same stoichiometry, for example, RP $Ba_2ZrO_4$ and the related $Ba_2ZrO_3F_2$ oxyfluoride share the same trait and have been shown to trap water molecules within their bulk.[17,18] Currently, the physical underpinnings of these properties are poorly understood because a number of important questions related to the adsorbates' entry to, motion through, and exit from the solid, including any specifics of the system structural and chemical changes during the molecular loading-unloading cycle, remain unanswered. Nevertheless, one can *speculate* that, due to the largeness of Ba ions, these compounds possess more open geometries (compared to the stoichiometrically similar Sr- and Ca-based structures), which may be connected to the observed unusual properties.

In this investigation, laying the groundwork for detailed studies of the solid interactions with small molecules, we probe structural, electronic, and vibrational properties of the monoclinic $P2_1/n$ $\beta$ phase of $Ba_2TiO_4$, with an emphasis on contrasting the influence of the unique, tetrahedral environment of the $Ti^{4+}$ cations with the more generic octahedral environment present in kindred perovskitelike compounds. A complementary investigation of the properties of a fictitious isostoichiometric RP $Ba_2TiO_4$ material subject to square epitaxial growth condition has been conducted as a separate project.[19] In Sec. II, we describe the key details of our computational approach based on density functional theory (DFT).[20] In Sec. III, the system relaxed lattice parameters and bond lengths, obtained by utilizing two different choices for the DFT exchange-correlation potential, are compared to experimental data. Section IV analyzes the electronic properties of $P2_1/n$ $Ba_2TiO_4$, including the charge-density-based evaluations of

 

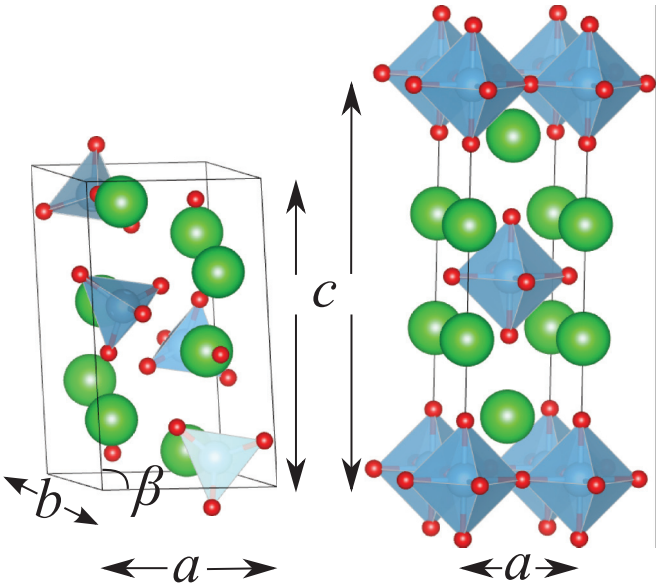


FIG. 1. (Color online) Unit cell and atomic positions of $P2_1/n$ $\beta$ (left) and $I4/mmm$ Ruddlesden-Popper (right) $Ba_2TiO_4$. Ba atoms are represented by the large green (light grey) spheres and sit between the translucent $TiO_n$ polyhedra. The lattice parameters for for both polymorphs are also shown. The off-90° angle $\beta$ between $c$ and $a$ highlights the monoclinic character of the $P2_1/n$ phase.

the relative sizes of Ba and Sr ions in $A_2TiO_4$ and $ATiO_3$ structures. Finally, in Sec. V, we investigate the stability of the $P2_1/n$ phase by calculating its vibrational spectrum and phonon band dispersions across the Brillouin zone (BZ) with density-functional perturbation theory (DFPT).[21] We also compute the electronic and phonon contributions to the static dielectric permittivity of $P2_1/n$ $\beta$-$Ba_2TiO_4$, evaluating its usefulness as a high-$\kappa$ material.

## II. COMPUTATIONAL DETAILS

All DFT calculations in this study utilize the QUANTUM ESPRESSO package[22] within the local density approximation (LDA), parameterized by Perdew and Zunger,[23] and the generalized gradient approximation (GGA) of Perdew, Burke, and Ernzerhof (PBE).[24] The electronic wave functions (density) are expanded in plane waves up to 30 Ry (300 Ry), and the core and valence electrons are treated with Vanderbilt ultrasoft[25] pseudopotentials.[26]

Shifted $4 \times 4 \times 4$ Monkhorst-Pack[27] meshes are used to integrate over the BZ of a twenty-eight-atom unit cell containing four $Ba_2TiO_4$ formula units (f.u.). All internal ionic positions are relaxed to forces of less than $0.4 \times 10^{-2}$ Ry bohr$^{-1}$ ($\sim$0.1 eV/Å). The phonon bands are calculated with DFPT by sampling the system dynamical matrices over a $4 \times 4 \times 2$ **q**-point BZ mesh. BZ paths used for displaying the phonon and electron band dispersions follow the conventions specified for monoclinic structures in Ref. 28. DFPT is also utilized to compute the ionic Born effective charge tensors $Z^*_{\alpha\beta}(i)$ [here, $i$ is the ion index and $\alpha,\beta$ are Cartesian directions $x,y,z$]. The methodology outlined in Refs. 29–32 is used to evaluate the effective phonon plasma frequencies $\Omega_{\text{eff}}$ and the static dielectric permittivity tensor $\epsilon_{\alpha\beta}(0)$. Finally, Bader analysis of the charge density[33–35] is employed to estimate relative ionic sizes of the cations in $P2_1/n$ $Ba_2TiO_4$ and other related compounds.

## III. STRUCTURAL PROPERTIES

The $P2_1/n$ $\beta$-phase of $Ba_2TiO_4$ has a monoclinic unit cell containing 28 atoms (four f.u.).[3,36] Figure 1 depicts the unit cells and atomic arrangements for both the $P2_1/n$ $\beta$ and RP $I4/mmm$ $Ba_2TiO_4$ polymorphs. The $TiO_4$ tetrahedra in the $P2_1/n$ phase appear to be more loosely packed in comparison with the arrangement of the $TiO_6$ octahedra in the $I4/mmm$ RP phase. The analysis of the polyhedral volumes presented in Sec. IV attempts to quantify the apparent difference in the structural openness of the two polymorphs.

### A. Lattice parameters

Table I shows the DFT-relaxed lattice parameters and the monoclinic angle $\beta$ in the $P2_1/n$ $\beta$-$Ba_2TiO_4$ structure and includes comparison to experimental data. As seen in other oxides (for example, in $BaTiO_3$[37–39]) LDA contracts lattice parameters with respect to experiment. GGA-PBE produces the closest match to experiment in $a$ and $c$ but underestimates $b$ and $\beta$. The addition of the $U$ parameter[40] to account for missing correlation in the LDA and GGA expands the PBE structure in every direction but simultaneously produces the value of $\beta$ that is closest to the one measured in experiment. These results illustrate the trend that DFT provides an accuracy in structural parameters to within a few percent of experimental measurements, but the exchange-correlation functional approximation makes it difficult to get systematically more accurate estimates.[41,42]

### B. Bond lengths

The values of average bond lengths computed for the $P2_1/n$ $\beta$-$Ba_2TiO_4$ structure with DFT are presented in Table II. Computational results obtained for the $I4/mmm$ RP structure, as well as comparisons to experimental measurements, are also included. For the $\beta$ phase, DFT simulation with LDA relaxes the short Ba-O bond length to 2.52 Å, close to the experimental values of 2.56–2.57[3,4] while the one utilizing GGA-PBE overshortens it to 2.39 Å. The experimental Ti-O bond length of 1.63 to 1.82 Å[3,4] is comparable to the LDA values of 1.78–1.81 Å while GGA-PBE predicts 1.81 to 1.85 Å. Charge density between Ti-O is increased in LDA with respect to

TABLE I. Structural parameters of $P2_1/n$ $\beta$-$Ba_2TiO_4$. All the lengths are given in angstroms, and the values of the monoclinic angle $\beta$ are given in degrees. Results of the experimental measurements are also included for comparison.

| | DFT | | | |
|---|---|---|---|---|
| | LDA | GGA(PBE) | GGA(PBE) + $U$[40] | Experiment[3,36] |
| $a$ | 6.040 | 6.128 | 6.221 | 6.096(4),6.12(3) |
| $b$ | 7.546 | 7.580 | 7.797 | 7.681(6),7.70(3) |
| $c$ | 10.340 | 10.461 | 10.698 | 10.545(9),10.50(3) |
| $\beta$ | 94.6 | 94.2 | 93.4 | 92.99(6),93.1(2) |

TABLE II. Bond lengths in the $P2_1/n$ $\beta$ and $I4/mmm$ RP $Ba_2TiO_4$ polymorphs computed with DFT. Results of experimental measurements for the $P2_1/n$ $\beta$ phase are also shown for comparison.

| | DFT | | |
|---|---|---|---|
| | LDA | GGA(PBE) | Experiment[3,4,36] |
| $P2_1/n$ | | | |
| Ba-O (Å) | 2.52–3.01 | 2.39–3.11 | 2.57-3.07, 2.57–3.23, 2.56–3.39 |
| Ti-O (Å) | 1.78–1.81 | 1.81–1.85 | 1.77-1.84, 1.77–1.84, 1.63–1.82 |
| O-O (Å) | 2.84–3.20 | 2.89–3.28 | . . . , . . . , 2.82–3.12 |
| $I4/mmm$ | | | |
| Ba-O (Å) | 2.70–2.79 | 2.67–2.82 | . . . |
| Ti-O (Å) | 1.95–1.97 | 1.98–1.99 | . . . |
| O-O (Å) | 2.78–2.79 | 2.81–2.82 | . . . |

GGA-PBE in both the $I4/mmm$ RP and $P2_1/n$ $\beta$ structures.[43] In other words, LDA fares better at relative ionic positions than at lattice parameters, and the opposite is true for GGA-PBE. Unlike the underbinding/overbinding behavior of LDA/GGA-PBE on lattice parameters, their relative predictions for bond lengths show no clear trend (see, for example, the internal parameter of both rutile and anatase $TiO_2$[44]). However, a comparison of several phases of BaO[45] shows stretching in LDA relative to GGA, in line with the sometimes smaller GGA-PBE Ba-O bond lengths in $\beta$-$Ba_2TiO_4$.

## IV. ELECTRONIC PROPERTIES

### A. Band gap

DFT calculations predict $\beta$-$Ba_2TiO_4$ to be a wide-gap insulator in both LDA and GGA-PBE. Table III presents Kohn-Sham energy band gaps at three combinations of BZ points while Fig. 2 shows the dispersions of LDA Kohn-Sham bands across a variety of symmetric directions in the BZ. The narrowest indirect gap lies between the valence-band maximum (VBM) at $H_1$ (midpoint of a BZ face edge) and the conduction-band minimum at $\Gamma$. The LDA indirect gap is smaller than the one obtained with GGA-PBE due to a more pronounced downward shift of a single low-lying state that forms the conduction-band minimum along the $\Gamma$-Y direction in the BZ. In other regions of the BZ, the LDA and GGA-PBE bands (latter not shown here) exhibit very similar behavior. Since DFT estimates of band gaps with either LDA or GGA-PBE are universally smaller than observed electronic band gaps,[46] we expect the measured gap of $\beta$-$Ba_2TiO_4$ to be greater than 4.5 eV. For comparison, the computed DFT-LDA band gap of the $I4/mmm$ RP phase is much smaller, only 1.75 eV.

TABLE III. Kohn-Sham band gaps in $P2_1/n$ $\beta$-$Ba_2TiO_4$.

| | LDA | GGA(PBE) |
|---|---|---|
| $\Gamma \rightarrow \Gamma$ | 4.265 | 4.589 |
| $H_1 \rightarrow \Gamma$ | 4.140 | 4.485 |
| $H_1 \rightarrow H_1$ | 4.509 | 4.499 |

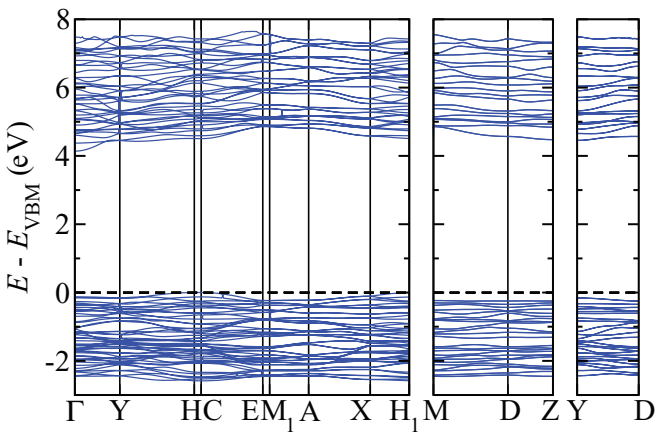


FIG. 2. (Color online) Electronic bands of the $P2_1/n$ $\beta$-$Ba_2TiO_4$ structure obtained with DFT-LDA. The indirect gap lies between the $H_1$ and $\Gamma$ points.

### B. Polymorph energetics

Energy comparison of the $Ba_2TiO_4$ polymorphs within the LDA places the $I4/mmm$ RP phase 0.220 eV/f.u. lower than the $P2_1/n$ $\beta$ phase. However, when GGA-PBE is used instead of LDA, the phase ordering is inverted, placing the energy of the $P2_1/n$ $\beta$ polymorph 0.301 eV/f.u. lower than that of the $I4/mmm$ RP one. The radical Ti coordination environment change—from tetrahedral in $P2_1/n$ to octahedral one in $I4/mmm$—between the two structures may be the source of the problem. Similar issues with the DFT description of polymorph energy ordering have been reported for other compounds, for example, $TiO_2$.[47] Although, in the case of $Ba_2TiO_4$, experimental data identifies $P2_1/n$ $\beta$ as the stable phase (which, nonetheless, forms *reluctantly* according to some experimental descriptions[6]), the sensitivity of this system to the choice of the exchange-correlation approximation in DFT does not completely resolve the issue of the degree of metastability of the $I4/mmm$ RP phase. If the RP phase energy is only slightly higher than that of the $\beta$ phase, it may be possible to stabilize the RP phase during a layer-by-layer growth with a square substrate since such conditions tend to promote the formation of perovskitelike structure. Naturally, a first-principles approach more accurate than DFT would be an attractive option for elucidating the energy ordering of the $Ba_2TiO_4$ polymorphs and determining whether the RP phase could be synthesized by an application of an epitaxial strain constraint.[19]

### C. Projected density of states

Continuing the evaluation of electronic properties of the $Ba_2TiO_4$ system within DFT, we compute the projected density of states (PDOS) in both polymorphs in order to understand how the changing coordination in the $TiO_n$ polyhedron affects the behavior of the electronic bands and the width of the resulting band gaps. Figure 3 depicts the ion-resolved PDOS for the $P2_1/n$ $\beta$ phase. As in other Ti-O systems, the PDOS shows that O $p$ states dominate at the top of the valence band manifold while the Ti $d$ states are most prominent at the bottom of the conduction band manifold. Calculations utilizing LDA or GGA-PBE (latter not shown) produce similar results.

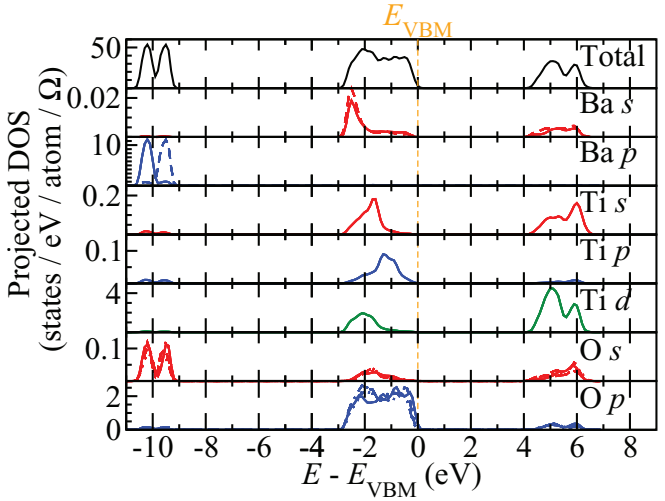


FIG. 3. (Color online) Projected density of states (PDOS) of $P2_1/n$ $\beta$-$Ba_2TiO_4$ computed with DFT-LDA. Dashed and dotted lines indicate contributions from same-element atoms at inequivalent Wyckoff positions. Notice different scales of the $y$ axis for different ion and electron subshell combinations.

PDOS of the $I4/mmm$ RP phase (not shown) exhibits the same general trends.

Comparison of the state-resolved PDOS for the Ti $d$ bands in $P2_1/n$ $\beta$ and $I4/mmm$ RP polymorphs reveals the effect of the octahedral versus tetrahedral arrangement of the surrounding O atoms as shown in Fig. 4. Our calculations for the $I4/mmm$ RP phase, presented in the lower panel of the figure, demonstrate that the distorted octahedral arrangement produces a large energy separation between the $t_{2g}$ and $e_g$ unoccupied states. Furthermore, some of the orbital symmetries are preserved by the distortion, and the $d_{xy}$ and $d_{zy}$ $t_{2g}$ states remain degenerate (the degeneracy between the $d_{z^2}$ and $d_{x^2-y^2}$ $e_g$ states is lifted, though). The observed trends are in agreement with the results of the molecular

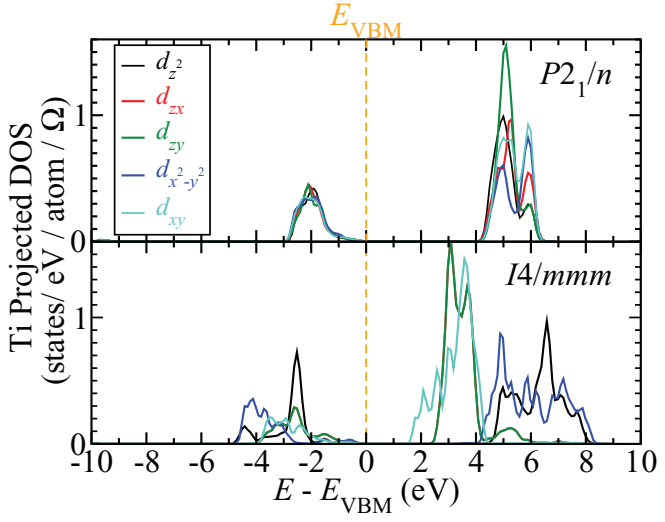


FIG. 4. (Color online) Projected density of states for Ti $d$ states in $P2_1/n$ $\beta$ and $I4/mmm$ RP $Ba_2TiO_4$. Section IV C addresses differences in symmetries of the $\beta$- and RP-phase PDOS.

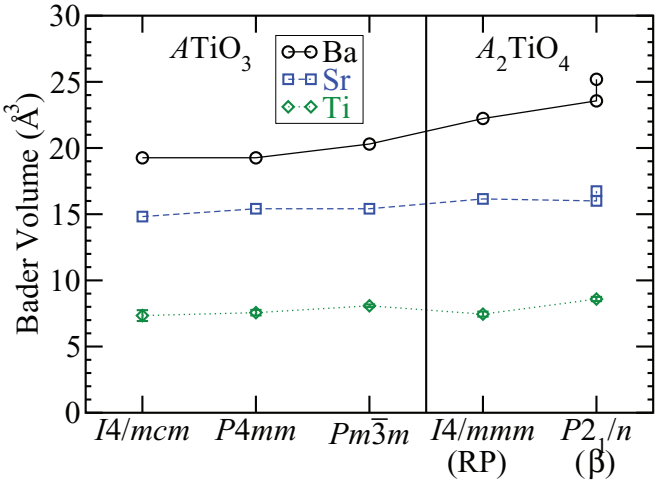


FIG. 5. (Color online) Bader volumes of Ba, Sr, and Ti ions in various $ATiO_3$ and $A_2TiO_4$ ($A$ = Sr, Ba) structures calculated with DFT-LDA. The Ti volumes do not change appreciably (i.e., by more than 1 Å$^3$) between the Ba- and Sr-based compounds, therefore only one curve is presented here. Two data points shown for Sr and Ba in the $P2_1/n$ $\beta$ structure represent Bader volumes of ions in distinct Wyckoff positions.

orbital theory analysis for the $TiO_6$ octahedron.[48] At variance, in the $P2_1/n$ $\beta$ phase, $TiO_4$ polyhedra are distorted away from ideal tetrahedral units[49,50] to such an extent that all of the orbital symmetries within the Ti $d$ band manifold are broken. Apparently, this allows for stronger mixing between these and the occupied O $2p$ states,[51,52] shifting the resulting unoccupied hybrids to higher energies compared to those in the $I4/mmm$ RP phase. At the same time, the tetrahedral distortions do not produce large splittings between the $d$ states, placing them at approximately the same energies. This makes their PDOS signatures—especially those within the occupied band manifold—barely distinguishable from one another. For example, in our calculations we cannot separate the splitting between the $1e$ and $2t_2$ occupied Ti $d$-O $p$ hybrid orbitals identified in the molecular orbital analysis of an ideal $TiO_4$ tetrahedron.[49,50]

### D. Bader and polyhedral volumes

In order to evaluate the relative "openness" of the two $Ba_2TiO_4$ polymorphs and to provide a comparison with $Sr_2TiO_4$ and the $ATiO_3$ ($A$ = Sr, Ba) compounds, we compute the cation Bader volumes and the volumes of the $TiO_n$ polyhedra for all of the aforementioned structures, shown in Fig. 5 and Table IV, respectively.

Figure 5 shows only values computed with DFT-LDA since GGA-PBE (not shown) produces volumes that differ less than 6% from the LDA results. These data indicate that the Bader volumes of Sr and Ti (the latter regardless of whether $A$ = Sr or Ba) remain practically constant in all the sampled structures. At the same time, the Bader volume of Ba, while much larger than that of Sr, dilates by 25% or 30% going from $BaTiO_3$ to $I4/mmm$ RP or $P2_1/n$ $\beta$ $Ba_2TiO_4$, respectively. The observed propensity of Ba to support a more open structural arrangement in the $A_2TiO_4$ stoichiometry may be an important

TABLE IV. $TiO_n$ polyhedron volumes $\Omega_{poly}$ (tetrahedra in the $P2_1/n$ and octahedra in all other structures), functional unit volumes $\Omega$ and their ratios in various $ATiO_3$ and $A_2TiO_4$ compounds calculated with DFT-LDA.

| | $\Omega_{poly}$ (Å$^3$) | | $\Omega$ (Å$^3$/f.u.) | | $\Omega_{poly}/\Omega$ (%) | |
|---|---|---|---|---|---|---|
| Symmetry | Sr | Ba | Sr | Ba | Sr | Ba |
| $ATiO_3$ | | | | | | |
| $I4/mcm$ | 9.6 | . . . | 56.9 | . . . | 16.9 | . . . |
| $P4mm$ | . . . | 10.7 | . . . | 61.4 | . . . | 17.4 |
| $Pm\bar{3}m$ | 9.5 | 10.2 | 57.1 | 61.0 | 16.6 | 16.7 |
| $A_2TiO_4$ | | | | | | |
| $I4/mmm$ | 9.6 | 10.1 | 90.4 | 102.1 | 10.6 | 9.9 |
| $P2_1/n$ | 3.8 | 3.9 | 101.9 | 117.4 | 3.7 | 3.3 |

factor promoting the stability of the loose $P2_1/n$ phase over the more closely packed $I4/mmm$ one preferred by the smaller Sr ions as pointed out by Bland from simple geometrical considerations.[3]

The polyhedron volume data assembled in Table IV for the same sampling of $ATiO_3$ and $A_2TiO_4$ structures provides a crude estimate of the relative openness of their geometries, e.g., with respect to accommodating small molecular species within the unit cell. Although the volume of the $TiO_6$ octahedron does not change in either Ba- or Sr-based structures upon transition from the $ATiO_3$ to $A_2TiO_4$ stoichiometry, the addition of the *interlayer gallery* in the latter expands the unit cell substantially, reducing the polyhedron-to-cell volume ratio from approximately 17 to 10%. However, this ratio falls even more dramatically—to ∼3.5%—in the transition to the $P2_1/n$ geometry since the volume of the tetrahedral $TiO_4$ unit is much smaller than that of the octahedral one. A f.u. volume comparison of the Ba- and Sr-based $A_2TiO_4$ polymorphs shows much larger volumes of the former, especially in the case of the $P2_1/n$ structure (15% expansion). However, a f.u. volume comparison of the (presumably) *stable* $I4/mmm$ $Sr_2TiO_4$ and $P2_1/n$ $Ba_2TiO_4$ polymorphs reveals an even stronger disparity, with the unit volume of the Ba-based structure being 30% larger.

These results show that both Ba-based $A_2TiO_4$ polymorphs possess more open geometries (the $P2_1/n$ $\beta$ phase more so than the $I4/mmm$ RP phase) than their isostoichiometric Sr-based counterparts and all of the examined $ATiO_3$ compounds. Therefore such Ba-based structures are attractive candidates for a variety of applications involving absorption and desorption of small molecules as already suggested by a number of experimental investigations.[14–18]

## V. VIBRATIONAL PROPERTIES

### A. Phonon bands

The calculated phonon bands of the $P2_1/n$ $\beta$-$Ba_2TiO_4$ structure and its corresponding vibrational density of states (VDOS) are shown together in Fig. 6. Phonon BZ dispersions for the $I4/mmm$ RP $Ba_2TiO_4$, including their dependence on the epitaxial strain, are presented and analyzed in Ref. 19. A few areas of relatively weak instabilities still present in the data of Figure 6 are most likely artifacts of the (still rather coarse) **q**-point BZ sampling in the DFPT dynamical matrix calculation.

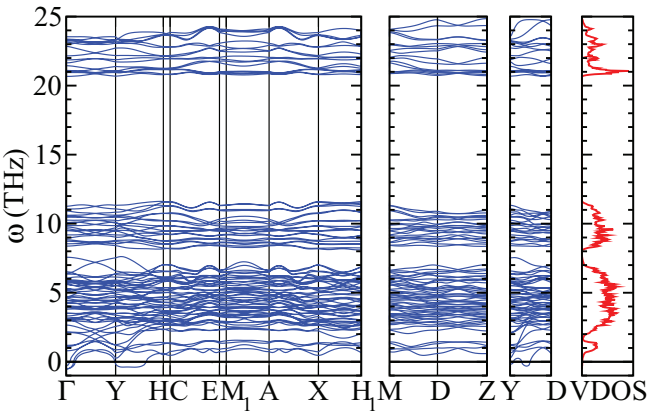


FIG. 6. (Color online) Phonon bands and vibrational density of states (VDOS) of the $P2_1/n$ $\beta$-$Ba_2TiO_4$ structure. Imaginary frequencies associated with unstable phonon modes are plotted as negative numbers below the zero line. A few weak instabilities still present in the structure are likely the result of the coarse BZ sampling in the dynamical matrix calculation. Phonon bands around 23 THz correspond to breathing modes of the $TiO_4$ tetrahedra observed by Raman spectroscopy.[53]

For a loose system such as $P2_1/n$ $\beta$-$Ba_2TiO_4$, with restoring forces being weak (associated energy landscapes—shallow) for some distortions, this is unsurprising. Visualization of the unstable mode eigenvector at Γ produces minor variations of the cell shape coupled with small rotations of the $TiO_4$ tetrahedra. In contrast, instabilities found in $I4/mmm$ RP $Ba_2TiO_4$ are much stronger, and further structural relaxations by following the associated eigenvectors result in phase transitions accompanied by substantial decreases of the system total energy.[19] Considering the small magnitudes of the unstable mode frequencies, we regard $P2_1/n$ $\beta$-$Ba_2TiO_4$ as being reasonably stable in DFT description, in agreement with the experimental observation of the $\beta$ phase predominance at low temperature. Having close to zero plasma frequencies (and therefore possessing no dipole moments), Γ-point instabilities are not included in the static dielectric permittivity tensor calculations in Sec. V B.

A Raman spectroscopic study of $\beta$-$Ba_2TiO_4$ found a peak near 745 cm$^{-1}$ (22.3 THz) attributed to symmetric vibration of the $TiO_4$ tetrahedra.[53] Among the calculated zone-center phonons, a Raman-active mode at 772 cm$^{-1}$ (23.1 THz) with $A_g$ symmetry consists primarily of symmetric O displacements around the Ti, Ba displacements being two orders of magnitude smaller.

### B. Born effective charges and static dielectric permittivity

The computed Born effective charge tensors $Z^*_{\alpha\beta}(i)$ are collected in Table V for both the $P2_1/n$ $\beta$ and $I4/mmm$ RP $Ba_2TiO_4$ polymorphs. Although, because of its low symmetry, the $\beta$ phase tensors for each ion have nonzero off-diagonal components, these components are small, and we do not show them in the table. Comparing the presented data with the effective charge tensors for $BaTiO_3$ computed within the same set of approximations,[54,55] we find that the in-plane charge tensor components for Ti and O(I-II) in the $I4/mmm$ RP structure remain anomalous, indicative of the

TABLE V. Born effective charges of $P2_1/n$ $\beta$- and $I4/mmm$ RP-$Ba_2TiO_4$ calculated in DFT-LDA. Off-diagonal terms of the $Z^*_{\alpha\beta}(i)$ ionic tensors in the $P2_1/n$ phase (not shown here) are one to two orders of magnitude smaller than the diagonal ones.

| | $P2_1/n$ | | | $I4/mmm$ | | |
|---|---|---|---|---|---|---|
| Ion | $Z^*_{xx}$ | $Z^*_{yy}$ | $Z^*_{zz}$ | $Z^*_{xx}$ | $Z^*_{yy}$ | $Z^*_{zz}$ |
| Ba(I) | 2.71 | 3.16 | 2.44 | 2.67 | 2.67 | 2.88 |
| Ba(II) | 2.77 | 2.66 | 3.00 | | | |
| Ti | 3.31 | 3.39 | 2.82 | 6.71 | 6.71 | 4.92 |
| O(I) | −1.38 | −3.65 | −1.52 | −5.30 | −2.19 | −1.59 |
| O(II) | −2.76 | −1.62 | −2.31 | −2.19 | −5.30 | −1.59 |
| O(III) | −2.88 | −2.07 | −1.70 | −2.29 | −2.29 | −3.77 |
| O(IV) | −1.82 | −1.91 | −2.78 | | | |

propensity towards a polar, or ferroelectric, phase transition. In contrast, none of the effective charges in the $P2_1/n$ $\beta$ structure have anomalous values, suggesting that small lattice distortions in $\beta$-$Ba_2TiO_4$ do not have any pronounced polar character.

Using data from the calculations of the Γ-point dynamical matrix eigenvalues and eigenvectors combined with the values $Z^*_{\alpha\beta}(i)$, we compute phonon contributions to the static dielectric permittivity tensor $\epsilon_{\alpha\beta}(0)$ in $P2_1/n$ $\beta$-$Ba_2TiO_4$.[29–32,56] Figure 7 shows the resulting effective plasma frequencies $\Omega_{\text{eff}}(\omega)$ for the $P2_1/n$ $\beta$ phase compared to those of the $I4/mmm$ RP phase.[19] The largest plasma frequency modes in the $P2_1/n$ structure have vibrational frequencies of 20.9, 21.0, and 21.7 THz (697, 702, and 724 $cm^{-1}$) with $B_u$, $A_u$, and $A_u$ symmetry, respectively, while, in the RP structure, such modes, in addition to having higher effective strengths, occur at much lower vibrational frequencies of 2.30, 2.35, and 11.5 THz (76.8, 78.2, and 384 $cm^{-1}$). Because individual

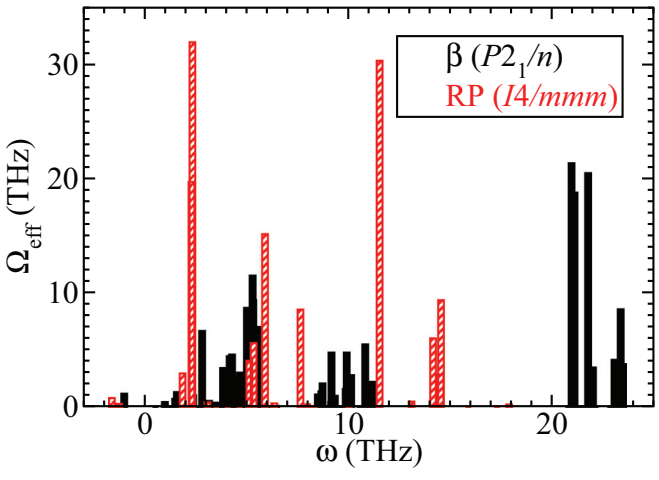


FIG. 7. (Color online) Effective plasma frequencies of Γ-point phonons in $P2_1/n$ $\beta$ and $I4/mmm$ RP $Ba_2TiO_4$ polymorphs. The $P2_1/n$ $\beta$ phase has only one vibrational mode with a relatively large plasma frequency ($\geqslant$10 THz) at a vibrational frequency of less than 10 THz, which results in weak phonon contribution to the static dielectric permittivity. In contrast, the $I4/mmm$ RP phase has numerous high-plasma/low-vibrational frequency modes.[19]

TABLE VI. Static dielectric permittivity of $P2_1/n$ $\beta$-$Ba_2TiO_4$ calculated with DFT-LDA and measured in experiment. The experimental value was measured on a 80% $\beta$-20% $\alpha'$ mixed-phase powder described in Ref. 11.

| | DFT-LDA | Exp.[11] |
|---|---|---|
| $\epsilon_\infty$ | (4.06,4.13,3.91) | ... |
| $\epsilon_0$ | (13.2,12.4,15.2) | ... |
| $\epsilon_{\text{av}}$ | 14 | 100 |

contributions of each vibrational mode $\xi_j$ to the phonon part of $\epsilon_{\alpha\beta}(0)$ scale as $\Omega^2_{\text{eff}}(\xi_j)/\omega^2(\xi_j)$, only modest values for the diagonal components of $\epsilon_0$, ranging from 12 to 15, result from our calculations for $P2_1/n$ $\beta$ phase (see Table VI for details). The situation is different in the $I4/mmm$ RP structure where in-plane values of $\epsilon_0$ in excess of 100 are predicted for a range of reasonable epitaxial strains.[19] To reconcile our findings with the results of experimental measurements that find an average $\epsilon$ value of 100 at finite and an even higher value at small frequencies,[11] we expect the largest contributions to the dielectric permittivity to be of non-phonon-related origin.

## VI. CONCLUSIONS

The low-temperature $P2_1/n$ $\beta$ phase of $Ba_2TiO_4$ is a monoclinic crystal with an unusual tetrahedral arrangement of the Ti-O bonds. DFT-based optimization of its structure produces lattice parameters and bond lengths accurate to within a few percent of the experimental values, depending on choice of exchange-correlation functional. Electronic properties evaluation shows that $\beta$-$Ba_2TiO_4$ is a wide band-gap insulator with Ti $d$ states dominating at the bottom of the conduction band and O $p$ states at the top of the valence band. DFT calculations of total energies with GGA-PBE favor the $P2_1/n$ $\beta$ phase over the $I4/mmm$ RP phase, but this relation is reversed when an LDA exchange-correlation functional is used instead of the GGA one. Therefore, more accurate electronic structure methods, such as DFT with hybrid exchange-correlation functionals or quantum Monte Carlo, should be employed to fully resolve the uncertainty concerning the lowest energy $Ba_2TiO_4$ polymorph and provide a more definite estimate of its electronic band gap. Bader analysis of the charge density confirms a larger ionic radius of Ba compared to Sr. This indicates that Ba supports a more open $A_2TiO_4$ structural arrangement, promoting the stability of the loose $P2_1/n$ phase over the more closely packed $I4/mmm$ phase. At the same time, comparison of the formula and $TiO_n$ polyhedral unit volumes of the 2-1-4 polymorphs shows that both Ba-based structures possess much more open geometries than their isostoichiometric Sr-based counterparts, in line with the demonstrated propensity of the Ba-based materials to capture molecules such as $CO_2$ and $H_2O$. However, the Born effective charges and the phonon contributions to the static dielectric permittivity tensor reveal an important difference in the behavior of $\beta$ and RP phases of $Ba_2TiO_4$: compared to the perovskitelike RP phase, the $\beta$ phase exhibits no strong polar character as indicated by both the nonanomalous values of its ionic Born effective charge tensor components and the

shift of the polar vibrational modes to higher frequencies. The combination of these factors leads to a rather low value of the average static dielectric constant in $\beta$-$Ba_2TiO_4$ (which in our calculations is estimated to be around 14) suggesting that non-phonon-related contributions may be responsible for the results obtained in experiments.[8,11]


## ACKNOWLEDGMENTS

This project was supported by the U.S. Department of Energy, Office of Science, Office of Basic Energy Sciences, and by American Recovery and Reinvestment Act (ARRA) funding through the Office of Advanced Scientific Computing Research under Contract No. DE-AC02-06CH11357.


*wparker@anl.gov


[1] D. E. Rase and R. Roy, J. Am. Ceram. Soc. **38**, 102 (1955).

[2] S. Lee, C. A. Randall, and Z.-K. Liu, J. Am. Ceram. Soc. **90**, 2589 (2007).

[3] J. A. Bland, Acta Crystallogr. **14**, 875 (1961).

[4] J. R. Günter and G. B. Jameson, Acta Crystallogr. Sect. C **40**, 207 (1984).

[5] S. N. Ruddlesden and P. Popper, Acta Crystallogr. **10**, 538 (1957).

[6] V. Shanker, T. Ahmad, and A. K. Ganguli, Bull. Mater. Sci. **27**, 421 (2004).

[7] T. Hungría and A. Castro, J. Alloys Compd. **436**, 266 (2007).

[8] G. Pfaff, J. Mater. Sci. Lett. **10**, 1059 (1991).

[9] G. Pfaff, J. Mater. Chem. **2**, 591 (1992).

[10] S. J. Lee, M. D. Biegalski, and W. M. Kriven, J. Mater. Res. **14**, 3001 (1999).

[11] T. Ahmad and A. K. Ganguli, J. Mater. Res. **19**, 2905 (2004).

[12] D. Guo, T. Goto, C. Wang, Q. Shen, and L. Zhang, Mater. Lett. **70**, 135 (2012).

[13] A. Ito, D. Guo, R. Tu, and T. Goto, Mater. Chem. Phys. **133**, 398 (2012).

[14] H. Marusawa and Y. Saito, Key Eng. Mater. **350**, 143 (2007).

[15] Y. Saito, H. Sato, and Y. Sakabe, J. Chem. Eng. Japan **41**, 441 (2008).

[16] R. Inoue, S. Ueda, K. Wakuta, K. Sasaki, and T. Ariyama, ISIJ Int. **50**, 1532 (2010).

[17] R. V. Shpanchenko, E. V. Antipov, and L. M. Kovba, Zh. Neorg. Khim. **38**, 599 (1993).

[18] P. R. Slater and R. K. B. Gover, J. Mater. Chem. **11**, 2035 (2001).

[19] W. D. Parker and S. M. Nakhmanson, Phys. Rev. B **88**, 035203 (2013).

[20] R. O. Jones and O. Gunnarsson, Rev. Mod. Phys. **61**, 689 (1989).

[21] S. Baroni, S. de Gironcoli, A. Dal Corso, and P. Giannozzi, Rev. Mod. Phys. **73**, 515 (2001).

[22] P. Giannozzi, S. Baroni, N. Bonini, M. Calandra, R. Car, C. Cavazzoni, D. Ceresoli, G. L. Chiarotti, M. Cococcioni, I. Dabo, A. D. Corso, S. de Gironcoli, S. Fabris, G. Fratesi, R. Gebauer, U. Gerstmann, C. Gougoussis, A. Kokalj, M. Lazzeri, L. Martin-Samos, N. Marzari, F. Mauri, R. Mazzarello, S. Paolini, A. Pasquarello, L. Paulatto, C. Sbraccia, S. Scandolo, G. Sclauzero, A. P. Seitsonen, A. Smogunov, P. Umari, and R. M. Wentzcovitch, J. Phys.: Condens. Matter **21**, 395502 (2009).

[23] J. P. Perdew and A. Zunger, Phys. Rev. B **23**, 5048 (1981).

[24] J. P. Perdew, K. Burke, and M. Ernzerhof, Phys. Rev. Lett. **77**, 3865 (1996); **78**, 1396 (1997).

[25] D. Vanderbilt, Phys. Rev. B **41**, 7892 (1990).

[26] For the LDA, the pseudopotentials have the following parameters: Ba: $5s^25p^66p^2$, $r_0 = 0.8$ bohr, $r_c^{\rm loc} = 1.8$ bohr, $r_c = (2.5,1.8)$ bohr for $s$, and $p$, respectively; Ti: $3s^23p^64s^23d^1$, $r_0 = 1.0$ bohr, $r_c^{\rm loc} = 1.8$ bohr, $r_c = (1.8,1.8,1.8)$ bohr for $s$, $p$, and $d$, respectively; O: $2s^22p^4$, $r_0 = 0.7$ bohr, $r_c^{\rm loc} = 1.0$ bohr, $r_c = (1.3,1.3)$ bohr for $s$ and $p$, respectively. For PBE, the Ba: $5s^25p^65d^06s^26p^0$, $r_0 = 1.3$ bohr, $r_c^{\rm loc} = 3.0$ bohr, $r_c = (2.6,2.0,2.2)$ for $s$, $p$, and $d$, respectively. The Ti pseudopotential has the same valence configuration and $r_c^{\rm loc}$ as for the LDA. The O pseudopotential has the same valence configuration and $r_c^{\rm loc}$ but $r_c = (1.2,1.2)$ a.u.

[27] H. J. Monkhorst and J. D. Pack, Phys. Rev. B **13**, 5188 (1976).

[28] W. Setyawan and S. Curtarolo, Comput. Mater. Sci. **49**, 299 (2010).

[29] G.-M. Rignanese, X. Gonze, and A. Pasquarello, Phys. Rev. B **63**, 104305 (2001).

[30] G.-M. Rignanese, F. Detraux, X. Gonze, and A. Pasquarello, Phys. Rev. B **64**, 134301 (2001).

[31] X. Zhao and D. Vanderbilt, Phys. Rev. B **65**, 075105 (2002).

[32] C. J. Fennie and K. M. Rabe, Phys. Rev. B **68**, 184111 (2003).

[33] G. Henkelman, A. Arnaldsson, and H. Jónsson, Comput. Mater. Sci. **36**, 354 (2006).

[34] E. Sanville, S. D. Kenny, R. Smith, and G. Henkelman, J. Comput. Chem. **28**, 899 (2007).

[35] W. Tang, E. Sanville, and G. Henkelman, J. Phys.: Condens. Matter **21**, 084204 (2009).

[36] K. K. Wu and I. D. Brown, Acta Crystallogr. Sect. B **29**, 2009 (1973).

[37] S. Tinte, M. G. Stachiotti, C. O. Rodriguez, D. L. Novikov, and N. E. Christensen, Phys. Rev. B **58**, 11959 (1998).

[38] D. I. Bilc, R. Orlando, R. Shaltaf, G.-M. Rignanese, J. Íñiguez, and P. Ghosez, Phys. Rev. B **77**, 165107 (2008).

[39] R. A. Evarestov and A. V. Bandura, J. Comput. Chem. **33**, 1123 (2012).

[40] G. Hautier, S. P. Ong, A. Jain, C. J. Moore, and G. Ceder, Phys. Rev. B **85**, 155208 (2012).

[41] L. Schimka, J. Harl, and G. Kresse, J. Chem. Phys. **134**, 024116 (2011).

[42] J. Sun, B. Xiao, and A. Ruzsinszky, J. Chem. Phys. **137**, 051101 (2012).

[43] See Supplemental Material at http://link.aps.org/supplemental/10.1103/PhysRevB.88.245108 for plots of charge density through various Ba-O and Ti-O bonds in $\beta$ and RP-$Ba_2TiO_4$.

[44] F. Labat, P. Baranek, C. Domain, C. Minot, and C. Adamo, J. Chem. Phys. **126**, 154703 (2007).

[45] R. G. Amorim, M. Verssimo-Alves, and J. P. Rino, Comput. Mater. Sci. **37**, 349 (2006).

[46] H. Dixit, R. Saniz, S. Cottenier, D. Lamoen, and B. Partoens, J. Phys.: Condens. Matter **24**, 205503 (2012), Fig. 1 plots the LDA or GGA gaps versus experiment for a large number of solids.

[47] M. E. Arroyo-de Dompablo, A. Morales-García, and M. Taravillo, J. Chem. Phys. **135**, 054503 (2011), see paragraph 1 of Sec. 3C and Fig. 6. Ti in rutile and anatase is sixfold coordinated but sevenfold coordinated in columbite.

[48] A. Koleżyński and K. Tkacz-Śmiech, Ferroelectrics **314**, 123 (2005).

[49] G. V. Ionova and M. E. Dyatkina, J. Struct. Chem. **6**, 128 (1965).

[50] A. J. Bridgeman and G. Cavigliasso, Polyhedron **20**, 2269 (2001).
[51] I. B. Bersuker, Ferroelectrics **164**, 75 (1995).
[52] I. B. Bersuker, *The Jahn-Teller Effect* (Cambridge University Press, Cambridge, UK, 2006).
[53] Y. S. Bobovich, Opt. Spectrosc. **13**, 274 (1962).
[54] P. Ghosez, X. Gonze, P. Lambin, and J.-P. Michenaud, Phys. Rev. B **51**, 6765 (1995).
[55] P. Ghosez, J.-P. Michenaud, and X. Gonze, Phys. Rev. B **58**, 6224 (1998).
[56] X. Gonze and C. Lee, Phys. Rev. B **55**, 10355 (1997).